LANGMUIR

pubs.acs.org/Langmuir Article

Durably Self-Sustained Droplet on a Fully Miscible Liquid Film

Yutian Shen, Jiyu Xu, Mingcheng Yang, Yongfeng Huang, Cui Zhang, Jiajia Zhou,* Kai Sun,* and Sheng Meng*

Cite This: *Langmuir* 2022, 38, 3993−4000 Read Online

ACCESS | Metrics & More | Article Recommendations | Supporting Information

ABSTRACT: Droplets impacting onto a solid or liquid surface inducing wetting, floatation, splash, coalescence, etc. is ubiquitous in nature and industrial processes. Here, we report that liquid droplets exhibit spherical caps upon contact with a fully miscible liquid film of lower surface tension, despite the spontaneous mixing of the two liquids. Such a spherical cap on a continuous liquid surface sustains a long lifespan up to minutes before ultimately merging into the film. Benefiting from large viscous forces in a thin film as a result of spatial confinement, the surface flow is substantially suppressed. Therefore, the surface tension gradient responsible for this phenomenon is maintained because the normal diffusion of film liquid into the droplet can timely dilute film liquid supplied by uphill Marangoni flow at the droplet surface. The present finding removes the conventional cognition that droplet coalescence is prompt on fully miscible continuous liquid surfaces, thus benefiting design of new types of microfluidic devices.

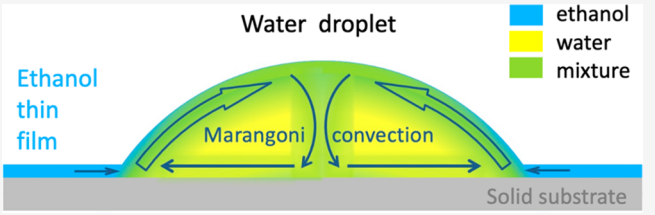

INTRODUCTION

Droplets are common in nature as rain drops and important in industrial as well as agricultural processes, including spray cooling, printing, lubrication, and irrigation.[1−21] Benefiting from its rapid heat and mass transfer[4] as a result of a high surface area to volume ratio, droplet is widely used to modify liquid transport[5−21] and improve mixing efficiency.[4,22,23] Volatile droplet can drive radical spreading in a water film underneath and even puncture it via a vapor-mediated Marangoni effect.[16−18] Droplets can spontaneously transport along certain directions.[5−15,19−21] Mixing within droplets can be enhanced via various techniques, including microfluidic channels[4,22] and introducing Marangoni convection,[23] thereby decreasing reaction times in chemical and biological synthesis.

On the surface of a solid or an immiscible liquid, droplets can sustain durably as a result of the balance between three different interfacial tensions.[12,24−28] On an imbibition film fed by droplet spreading on a rough solid surface, where solid and liquid coexist, a transient droplet can exist before complete loss into the microtexture.[29,30] If a droplet is deposited on a continuously miscible liquid surface, however, the liquid−liquid interface between the droplet and the reservoir disappears immediately upon contact. The merged liquid−gas surface promptly deforms to minimize the surface energy, although the coalescence process may contain a cascade of pinch-offs.[31−38] To the best of our knowledge, the only way to retard coalescence on a continuously miscible liquid reservoir is to manipulate the gas film between the approaching liquid surfaces via complete and subtle operations, such as vibration of the liquid reservoir,[39] well-controlled temperature difference between the droplet and the reservoir,[40,41] and addition of a surfactant.[42]

Here, we report that a liquid droplet can maintain a self-sustained spherical cap for up to minutes shortly after coalescing with a continuous liquid film of full miscibility and lower surface tension, despite simultaneous mixing. Restricted by the large viscous forces in the liquid film, the Marangoni convective transport of film liquid into the droplet tangential to the surface is substantially suppressed. If its magnitude is comparable to the diffusion of film liquid into the droplet normal to the surface, a certain mixture fraction difference can be established and maintained along the droplet surface; thus, the corresponding surface tension difference maintains the droplet. This phenomenon with a spontaneously durable spherical cap shape on a miscible liquid surface and Marangoni convection provides a novel type of microfluidic system.

EXPERIMENTAL SECTION

The thin liquid film is blade-coated[43] using the blade coater PF 400-H from Schwan Technology on a glass slide. Blade coating can efficiently help film liquid of low surface tension spread as a result of the pinning effect[44−47] from contamination or roughness of the solid surface. The thickness of the thin film is assumed the width of the slit. Glass slides

Received: December 27, 2021
Revised: March 14, 2022
Published: March 25, 2022

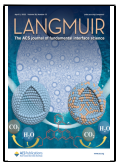

https://doi.org/10.1021/acs.langmuir.1c03457
Langmuir 2022, 38, 3993−4000

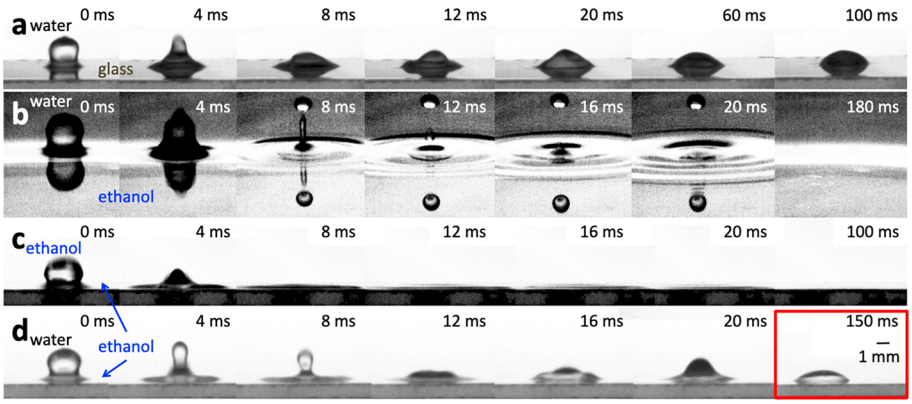

Figure 1. Formation of the spherical cap water droplet on a fully miscible ethanol film. (a) Water deposited onto a solid glass (impacting velocity of 0.06 m/s). (b) Water droplet merges into an ethanol pool (thickness of the pool of 8 cm and impacting velocity of 0.08 m/s). (c) Ethanol droplet merges into an ethanol film on glass (film thickness of 50 μm, impacting velocity of 0.10 m/s, and 0 °C). (d) Water droplet deposited on an ethanol film on glass. The red box shows the spherical cap shape of the droplet (film thickness of 50 μm, impacting velocity of 0.13 m/s, and 0 °C).

(Shunfei Microscope Slides 7101) taken directly from the box were used within 2 min as a solid substrate in Figure 1a and under thin films. The substrate in Figure 2 is a SiO_2/Si wafer. The gray solid substrate in Figure 4c and Figures S2 and S7 of the Supporting Information is aluminum foil freshly opened and covered by an ethanol film in 2 min.

The high-speed photos in Figure 1 are taken by pco.dimax HD. Photos in Figures 2 and 4c and Figures S2 and S7 of the Supporting Information are taken by Canon 7D, where the orange droplets are water-dyed by methyl orange for easy viewing. The impacting velocities in Figure 1 are detected by adjacent photos. Those in Figure S2 of the Supporting Information are controlled by the height of free fall, ignoring the slight velocity out of the pipetting gun. The temperature is controlled by the variable temperature holder DataPhysics TC/TPC 150.

The (apparent) contact angles were read from side views of droplets taken by DataPhysics OCA 20 using software SCA20_U. The initial apparent contact angles were measured on the earliest frames (the time interval of adjacent frames is 34 ms) when clear spherical caps emerge, about hundreds of milliseconds after the depositions.

RESULTS AND DISCUSSION

We first show three types of known phenomena. In Figure 1a, a water droplet deposited onto a solid surface (glass substrate) shows a typical and durable spherical cap in partial wetting. In Figure 1b, a water droplet deposited onto an ethanol pool results in partial coalescence within 20 ms,[32,48] and the complete merge can be observed at 180 ms. Figure 1c shows an ethanol droplet dripped onto a thin film of the same liquid. Although the mobility of the liquid is suppressed by the large viscous force in a thin film,[33,34,49] the merged surface still flattens within 8 ms and completely merges in 100 ms, which results from minimization of the surface energy of liquid ethanol.

If a water droplet (7 μL of water) is deposited on a thin ethanol film, as shown in Figure 1d, we observe unexpected results. Specifically, the merged surface substantially deforms within 12 ms, whereafter it oscillates less intensively and turns into a spherical cap shape at 150 ms. Water and ethanol keep in contact without an air cushion. The upper surface of this system is a completely continuous liquid without participation of solid. Such morphology is similar to the partial wetting on solid substrates, and its lifetime can reach several minutes at 0 °C. Figure 2 shows such a spherical cap droplet on an ethanol film supported on a silica wafer. This phenomenon also exists if ethanol is replaced by methanol, 1-propanol, or isopropanol.

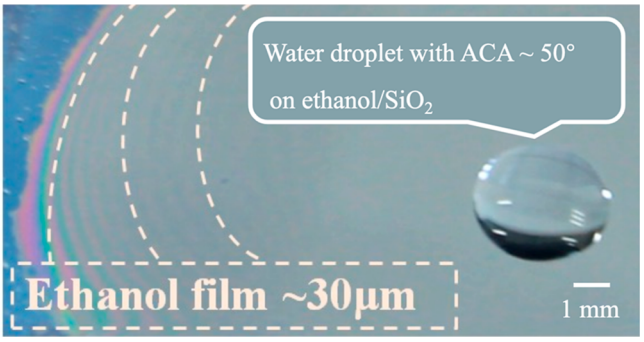

Figure 2. Image of a spherical cap water droplet on an ethanol film. The ethanol film is on a silica wafer. Dash circles show interference rings because of interference between reflectional lights from the upper and lower surfaces of the thin film.

To quantify such spherical cap configuration, the "apparent contact angle" (ACA) of the newly formed spherical cap water droplet on an ethanol film in Figure 1d is measured as approximately 50°. The spherical cap morphology gradually flattens as the mixing of two liquids proceeds; therefore, the initial ACA can also be labeled as ACA_{max}. ACA_{max} of the water droplet (10 μL) on a thin film of methanol, ethanol, 1-propanol, or isopropanol (thickness of 50 μm) is all around 50° (Figure S1 of the Supporting Information).

Such a spherical cap droplet on a miscible thin film is very robust, and ACA_{max} is little affected by the impact inertia. Even at a large impacting velocity of 2.5 m/s, although the droplet initially spreads more widely on the film, it soon retracts and a quasi-steady spherical cap can be formed (Figure S2a of the Supporting Information). Extensive experiments with the Weber number ($We = \rho R_0 v^2/\gamma_0$, where v is the impacting velocity and ρ, R_0, and γ_0 are the density, radius, and surface tension of the droplet as a sphere before deposition, respectively) ranging from 0.73 to 18.37 show only a slight variation of ACA_{max} within 10° (Figure S2b of the Supporting Information). Linear extrapolation to a We number of 0 gives an initial apparent contact angle of 56.5°. This indicates that the spherical cap configuration is a quasi-equilibrium state independent of the impact condition, which, therefore, should

https://doi.org/10.1021/acs.langmuir.1c03457
Langmuir 2022, 38, 3993−4000

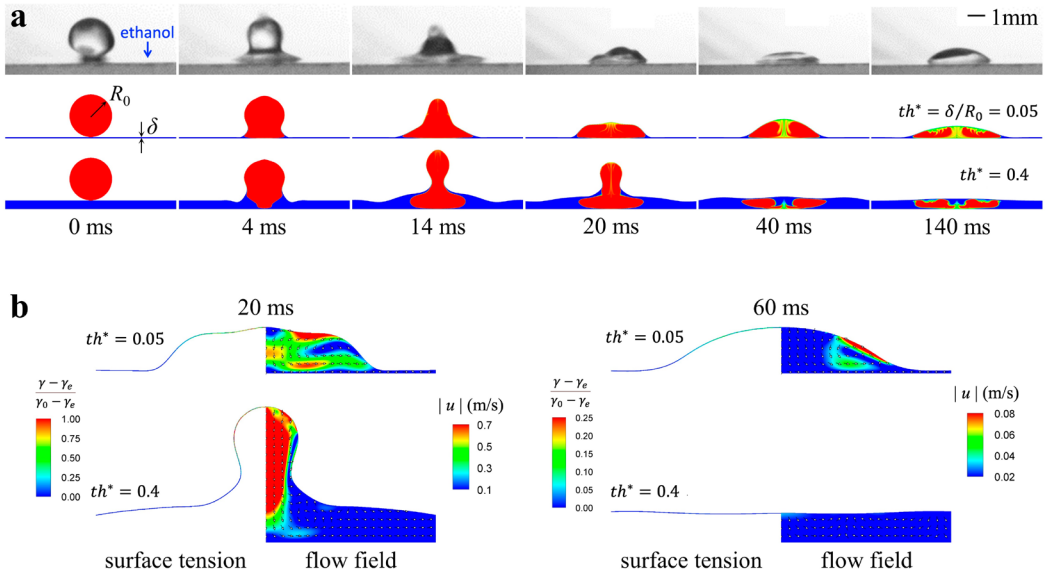

Figure 3. Simulation of droplet formation. (a) Experimental (first row, $\gamma^* = 0.3$, $Sc = 1000$, $Oh \sim 0.005$, impacting velocity = 0.12 m/s, and $th^* = 0.05$) and simulated (second row) side views of water droplet formation on a thin ethanol film. For comparison, water merges into a thick ethanol film in the simulation (third row). In simulations, $\gamma^* = 0.3$, $Sc = 1000$, $Oh \sim 0.014$, and the impacting velocity is 0 m/s. The radius of the droplet as a sphere before deposition R_0 and the thickness of film δ are labeled by black arrows. The red color fluid donates water, blue is for ethanol, and intermediate colors are for the mixture. (b) Evolution of surface tension (left side) and flow field (right side), where arrows indicate the flow direction.

be dominated by the intrinsic physical properties of this microfluidic system. The vapor of ethanol is also insignificant because the droplet formation process is comparable at 0 °C (Figure 1d) and room temperature (Figure 3a). Additionally, ACA_{max} is also comparable from 0 to 40 °C (Figure S3 of the Supporting Information) as the statured vapor pressure of ethanol increases over 10 times.

To understand the self-sustaining mechanism of the spherical cap droplet, we numerically simulated (for numerical methods, see the Supporting Information) the coalescence of a droplet with a film of lower surface tension liquid (Figures S4 and S5 of the Supporting Information). To focus on the intrinsic surface tension difference between the droplet and the film, we neglect the density and viscosity disparities between the two liquids as well as the initial impact velocity. The gravity effect is not taken into account because $Bo = \Delta\rho g R_0 \delta/\gamma \ll 1$, where $\Delta\rho = \rho - \rho_{gas}$, δ is the film thickness, and γ is the surface tension of liquid. Therefore, according to scaling analysis, such a simplified system can be described by six independent dimensionless parameters, including the surface tension ratio $\gamma^* = \gamma_{film}/\gamma_0$, the ratio of the film thickness to droplet radius $th^* = \delta/R_0$, the Ohnesorge number $Oh = \mu/\sqrt{\rho\gamma R_0}$ (where μ is the viscosity of liquid), the Schmidt number $Sc = \mu/\rho D$ (where D is the diffusion coefficient), the liquid−gas density ratio ρ^*, and the liquid−gas viscosity ratio μ^*. In our simulations, we take impacting velocity = 0 m/s, $\gamma^* = 0.3$ for water deposited onto ethanol, $Sc = 1000$, $\rho^* = 500$, and $\mu^* = 50$ for typical values of a liquid−gas system. To alleviate the tremendous computational demand in resolving the thin ethanol film, we used a film thickness ($th^* = 0.05$) slightly larger than the experiment ($th^* = 0.02$) and an increased Oh number of 0.014 (experimental $Oh \sim 0.005$) to compensate for the associated reduction of viscous stress $\mu U_{Ma}/\delta$ in the film, where U_{Ma} is the speed of Marangoni flow discussed later. Another case with a much thicker film of $th^* = 0.4$ was also simulated for comparison.

As shown in Figure 3a, our simulation with a thin film ($th^* = 0.05$) successfully reproduced the emergence of the spherical cap droplet, while a thick film ($th^* = 0.4$) yields full encapsulation of the droplet into the film. Two prominent differences were also observed. First, droplet deformation is more intensive on the thicker film, and the apex of the droplet rises up higher at 14 ms. Second, mixing of the two liquids is more efficient on the thinner film, because a broader mixing region (colored yellow) can be observed in the spherical cap droplet at 40 and 140 ms. The thin film around the droplet remains pure ethanol.

In this regard, we note that the surface tension difference between the ethanol film and the water droplet is large. The Marangoni effect or, more specifically, the converging fluid motion that the ethanol film tends to wrap up the water droplet could substantially affect the coalescence process. By furthering into the surface tension distribution and the flow field (Figure 3b), we observe a surface tension gradient along the droplet surface as well as the associated Marangoni flow (red region near the surface in the velocity field) at 20 ms for both cases. At 60 ms, however, the surface tension gradient and the Marangoni flow can be only observed in the thin film case, while in the thick film case, the surface has flattened with a uniform surface tension of ethanol. This implies that the Marangoni flow is necessary for the durable spherical cap droplet, and the self-sustaining surface tension gradient along the droplet surface is the root cause of this phenomenon.

In the present binary-liquid system, the surface tension of the droplet is determined by the mass fraction of the lower surface tension liquid from the film (i.e., ethanol) (Figure S6 of the Supporting Information). The film liquid at the droplet surface is supplied by the tangential convective ethanol flux. At the same time, ethanol at the droplet surface is in contact with water in the droplet. Normal diffusion between outer ethanol and inner water decreases the ethanol fraction at the surface. Therefore, it is reasonable to expect that a certain surface

https://doi.org/10.1021/acs.langmuir.1c03457
Langmuir 2022, 38, 3993−4000

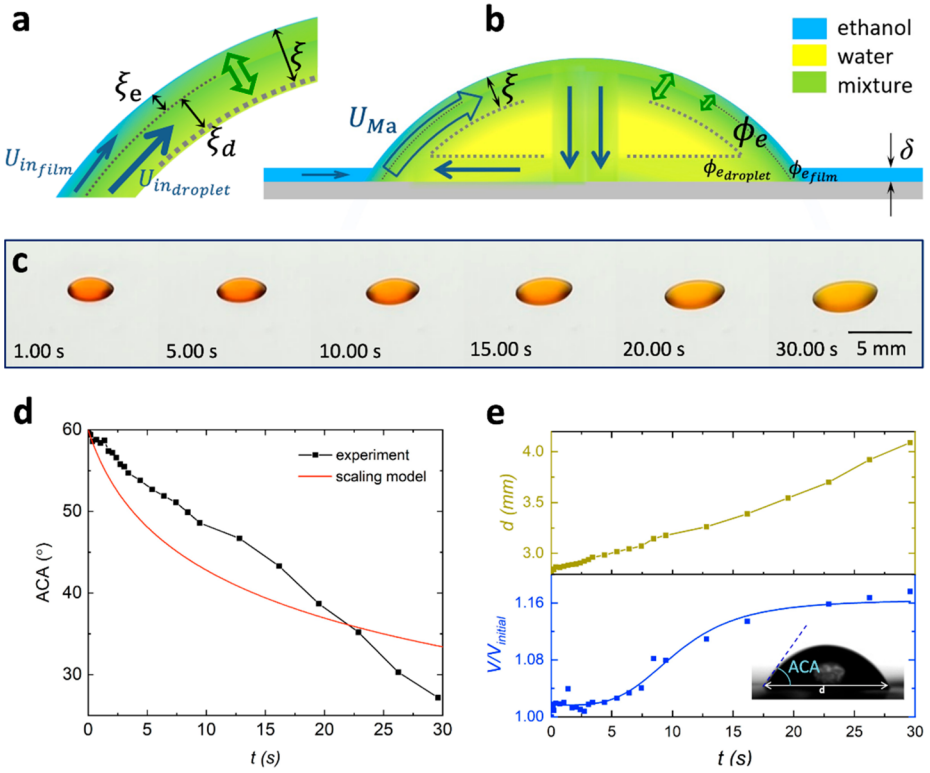

Figure 4. Evolution of a spherical cap droplet on a fully miscible film. (a) Diagram of the surface fluid layer entrained by the Marangoni flow, of which the thickness is ξ and the speed is U_{Ma}. It is composed of both the flow from the thin film at the outer layer (thickness ξ_e and speed $U_{in_{film}}$) and the flow from the water droplet at the inner layer (thickness ξ_d and speed $U_{in_{droplet}}$). As for the colors, yellow, blue, and intermediate colors represent water, ethanol, and mixtures, respectively. The normal diffusion between the outer layer and the inner layer is indicated by a green hollow arrow. (b) Diagram of the simplified Marangoni convection (left side where the blue arrows indicate the flow direction) and distribution of the ethanal fraction (right side where the green hollow arrows indicate a normal diffusion). ϕ_e is the ethanol fraction in the surface layer. The ethanol fractions of the outer layer and the inner layer are $\phi_{e_{droplet}}$ and $\phi_{e_{film}}$, respectively. (c) Stable colored water droplet on a thin ethanol film for half a minute ($\gamma^* = 0.3$, $th^* = 0.03$, and $Oh \sim 0.005$). (d) Evolution of the apparent contact angle (ACA) detected and predicted by scaling analysis. (e) Evolution of the diameter at bottom d (labeled in the inset) and the volume (calculated as the volume of the spherical cap using the detected ACA and d) of the droplet. The detected data are from the same process ($\gamma^* = 0.3$, $th^* = 0.03$, $Oh \sim 0.005$, and 0 °C). The impacting velocity is 0.10 m/s.

tension gradient can be durably sustained on the droplet surface only if the diffusive water flux can be supplied to the surface during the Marangoni "wrap up" process. Otherwise, the droplet surface would be covered by pure ethanol upon completion of "wrap up", and the spherical cap droplet cannot be sustained with a uniform surface tension of ethanol. In view of this, we shall compare the two independent time scales, namely, the characteristic time for the convective Marangoni "wrap up" process t_1 and the characteristic time for the diffusive dilution of ethanol normal to the surface t_2.

To estimate t_1, we note that the speed of Marangoni flow can be derived through balancing the Marangoni stress $\Delta\gamma/R_0$ and the viscous stress $\mu U_{Ma}/\xi$ as $U_{Ma} \sim \xi\Delta\gamma/R_0\mu$. Here, ξ denotes the fluid layer thickness that is entrained by the shear flow in the direction counter-radically tangential to the spherical cap (the surface layer colored both red and green in the velocity field at 60 ms in Figure 3b, schematically shown in panels a and b of Figure 4) (we introduce ξ instead of using the height of the droplet to obtain U_{Ma} in consideration that radically spreading flow at the bottom coexists with this shear flow in the droplet, and the Marangoni stress can only drive the later at the surface). ξ can be estimated by $\xi \sim \sqrt{\mu t_{osc}/\rho} \sim R_0\sqrt{Oh}$, in which $t_{osc} \sim \sqrt{\rho {R_0}^3/\gamma}$ is the capillary-driven oscillation time of the droplet. ξ is calculated as 0.4 mm using the experimental Ohnesorge number of 0.005, which matches well with the thickness of the simulated surface layer in Figure 3b as the reproduction of the experiment in Figure 3a. Therefore, $U_{Ma} \sim \sqrt{Oh}\,\Delta\gamma/\mu$. Then, t_1 can be obtained by $t_1 \sim \pi R_0/U_{Ma} \sim \pi R_0\mu/\sqrt{Oh}\,\Delta\gamma$.

To estimate t_2, we note that the surface layer of the droplet entrained by the Marangoni flow is composed of both the flow from the thin film at the outer layer and the flow from the water droplet at the inner layer. As schematically illustrated in Figure 4a, $\xi = \xi_e + \xi_d$, where ξ_e and ξ_d are the thickness of the outer layer and the inner layer, respectively. At the droplet surface, the viscous stresses of the outer layer and the inner layer are $\mu U_{in_{film}}/\xi_e$ and $\mu U_{in_{droplet}}/\xi_d$, respectively, where $U_{in_{film}}$ and $U_{in_{droplet}}$ are the speeds of the counter-radically incoming liquid in the thin film and droplet. In either the inner or outer layer, viscous stress is balanced by the same Marangoni stress $\Delta\gamma/R_0$; thus, $U_{in_{film}}/U_{in_{droplet}} \sim \xi_e/\xi_d$. At the rim of the droplet where liquid flows from the film into the droplet, the viscous stresses in the film side and the droplet side must be continuous. By balancing the viscous stresses in the ethanol film and the droplet $U_{in_{film}}/\delta \sim \mu U_{in_{droplet}} R_0$, we have $U_{in_{film}}/U_{in_{droplet}}$

https://doi.org/10.1021/acs.langmuir.1c03457
Langmuir 2022, 38, 3993−4000

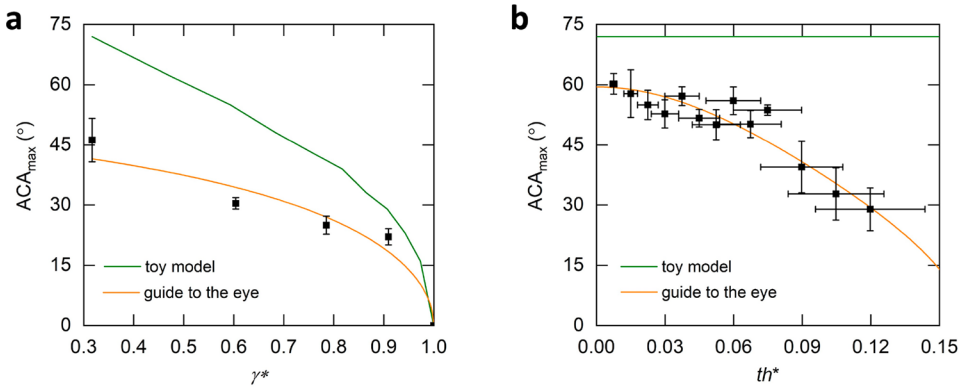

Figure 5. Initial apparent contact angles (ACA_{max}) of aqueous droplets on a miscible film. (a) ACA_{max} of aqueous droplets at various surface tension ratios (th^* = 0.07, and Oh ranges from 0.005 to 0.009 as the droplet concentration varies). Toy model prediction (green line) considers only surface tension without diffusion. (b) ACA_{max} of water droplets at various normalized thicknesses (γ^* = 0.3, and $Oh \sim 0.005$).

$\sim \delta/R_0$. Therefore, $\xi_e/\xi_d \sim \delta/R_0 = th^*$. ξ_e could be substantially suppressed if th^* is small. The characteristic thickness of the ethanol convective flux over the droplet surface is $\xi_e \sim \xi\delta/(\delta + R_0) \sim \sqrt{Oh}\,\delta R_0/(\delta + R_0) \sim \delta\sqrt{Oh}$. Therefore, the characteristic time scale for normal diffusion (green hollow arrows in panels a and b of Figure 4) t_2 can be estimated by $t_2 \sim \xi_e^2/D \sim \delta^2 Oh/D$.

By comparing these two time scales, we have

$$\frac{t_2}{t_1} \sim \frac{\delta^2 Oh}{D}\frac{\sqrt{Oh}\,\Delta\gamma}{\pi R_0 \mu} \sim Sc(1-\gamma^*)th^{*2}/Oh^{1/2} \quad (1)$$

To maintain a durable surface tension gradient on the droplet surface, t_2/t_1 must be relatively small, so that the inner water beneath the ethanol layer can readily diffuse to the surface. We can also have $t_2/t_1 \sim PeOhth^{*2}$, because the Sc number can be replaced by $Sc = Pe/Re$, with the Reynolds number $Re = \rho U_{Ma} R_0/\mu = (1-\gamma^*)/Oh^{3/2}$. It indicates that the present phenomenon fundamentally requires a small Pe; namely, the diffusional transport is relatively fast compared to the convective transport. For the present water−ethanol experiments with $Sc \sim 10^3$, $\gamma^* = 0.3$, and $Oh = 0.005$, this fundamentally requires th^* to be smaller than 0.2 according to our observations when the spherical cap becomes hard to distinguish. The configuration of the spherical cap is judged by the naked eyes with an approximate critical film thickness of about $th^* = 0.2$. The present observation gives a maximum t_2/t_1 of $O(10^2)$ for reference. Two distinct cases with and without the spherical cap at different th^* in the experiment (panels b and d of Figure 1) and simulation (Figure 3), together with all cases for non-zero ACA_{max} detections (Figure 5b and Figures S1−S3 of the Supporting Information), are consistent with this value.

Because the mixing process continues until homogeneity, the droplet should finally merge into the infinitely vast liquid film. Surprisingly, this water droplet on the ethanol film can exist for minutes (Figure 4c and Figure S7 of the Supporting Information) without breakup of the liquid film (for comparison, a droplet with a dry edge partially disconnecting an ethanol film is shown in Figure S7 of the Supporting Information). For the water droplet on an ethanol thin film ($\gamma^* = 0.3$, $th^* = 0.03$, $Oh \sim 0.005$, $Sc = 1000$, and 0 °C), its apparent that the contact angle gradually decreases to half of the initial value after 30 s (Figure 4d). Meanwhile, the diameter at the bottom of spherical cap d and the volume of the droplet V (calculated as the volume of the spherical cap using the detected ACA and d) increase (Figure 4e), indicating that a certain amount of ethanol in the film is transported into the droplet via surface flow.

Longevity of the self-sustained spherical cap droplet indicates a simultaneously sustained surface tension gradient with normal diffusion consistently consuming the wrapping-up ethanol, of which the flux is substantially restrained by large viscous stress in the thin film. As mixing precedes, the decreasing surface tension gradient along the droplet surface leads to a lower speed of liquid transport and, thus, a lower decreasing rate of the surface tension gradient, presenting a negative feedback that can durably maintain the spherical cap droplet for up to minutes.

After convergence at the apex of the droplet, the surface flow diverts downward to the bottom and then spreads outward before climbing up with the Marangoni flow again. This can be simplified as a donut-like circular convection within the spherical cap droplet, where liquids from the inner layer and the outer layer keep normal diffusion (Figure 4b). The span of each circle is ∼0.1 s with the droplet size of a few millimeters and the speed of Marangoni flow of ∼0.1 m/s (simulation in Figure 3b), which is small compared to the evolution process of the droplet up to minutes. Therefore, the evolution of the droplet can be modeled as a succession of quasi-steady flow circles, during which the speed of Marangoni flow is assumed as a constant and the evolution time t of the spherical cap configuration is the sum of all previous spans. The span of each circle Δt is estimated as $\Delta t \sim \pi R_0/U_{Ma}(t)$, which gradually increases as U_{Ma} decreases.

The ACA is determined by surface tension of the droplet $\gamma(\phi_e)$ via Young's equation $\gamma_e/\gamma(\phi_e) = \cos ACA$. The surface tension at the film side is the surface tension of pure ethanol γ_e based on two considerations: the thin film around the droplet fluid remains pure ethanol according to the simulation, and ethanol in the film is unidirectionally transported into the droplet because the volume of the droplet experimentally increases. The surface tension at the droplet side $\gamma(\phi_e)$ is assumed constant at the droplet surface, ignoring the distribution, as shown in Figure 3b. This assumption is made to support feasibility to analyze ACA in scaling arguments. $\gamma(\phi_e)$ can be fitted from the ethanol fraction in the surface layer (thickness ξ) of the droplet $\phi_e(t)$ using experimental data (Figure S6 of the Supporting Information). The fluid within the surface layer is composed of both the inner layer and the

https://doi.org/10.1021/acs.langmuir.1c03457
Langmuir 2022, 38, 3993−4000

outer layer (Figure 4b). The ethanol fraction of the inner layer $\phi_{e_{droplet}}$ gradually increases. The ethanol fraction of the outer layer $\phi_{e_{film}}$ equals 1 because the outer layer is from the thin film of pure ethanol. Using the relationship $\xi_e \sim \xi\delta/(\delta + R_0)$, we obtain $\phi_e(t) \sim [\phi_{e_{film}}(t)\delta + \phi_{e_{droplet}}(t)R_0]/(\delta + R_0)$ as the spatial average.

Diffusion between the inner layer and the outer layer in each circle starts from the uphill surface flow at the rim of the droplet and continues along the circular flow. In the newly formed spherical cap, the outer layer and the inner layer are perfectly mixed when the convection returns to the rim of the droplet according to the simulation in Figure 3a. The speed of diffusion is a constant determined by the diffusion coefficient, while the span of the circular flow gradually increases. Therefore, the inner layer and the outer layer must be well-mixed at the end of each circular convection afterward. Two fluids are assumed perfectly mixed when the next circle starts; i.e., $\phi_{e_{droplet}}(t) \sim \phi(t - \Delta t)$. Therefore, the temporal ethanol fraction at the rim of the spherical cap droplet can be estimated by

$$\phi_e(t) \sim \frac{\phi_{e_{film}}(t)\delta + \phi_e(t - \Delta t)R_0}{\delta + R_0} \quad (2)$$

The experimental $ACA_{max} \sim 60°$ gives $\Delta\gamma(t = 0\ s) \sim 46$ mN/m via Young's equation. We then artificially chose $th^* = 0.0025$ referring to the value of Marangoni speed in simulation $U_{Ma}(t = 0\ s) \sim 0.10$ m/s (here, the formation time of 0.14 s is ignored in comparison to the evolution for minutes) and that in the model $U_{Ma} \sim \delta\Delta\gamma/R_0\mu$ (here, we use δ rather than ξ to account for the large viscous force in the thin film, which is consistent with the self-sustaining mechanism and the simulation). Using $\pi R_0 \sim 3$ mm referring to the diameter at bottom of the droplet, the evolution in the scaling model successfully reproduces the slowly decreasing ACA (Figure 4d).

The value of th^* smaller than the experiment (0.03) may root from both aspects of the model and the experiment. From the aspect of the model, surface tension at the droplet surface is assumed as a constant, ignoring the spatial distribution to support feasibility to analyze ACA in scaling arguments. Such simplification overestimates $\Delta\gamma$ at the droplet rim and predicts a larger U_{Ma}; thereby, th^* in the model needs to be small for composition. From the experimental aspect, th^* gradually deceases because the film thickness actually decreases with ethanol entering the droplet and evaporation that may not be ignored in the long evolution process for 30 s.

A lower th^* leads to a lower decreasing speed of ACA (Figure S8 of the Supporting Information). Small th^* indicates a small spatial contribution of ethanol from the outer layer to the droplet surface and limited flow speed as a result of large viscous forces. Therefore, the increase of the ethanol fraction at the droplet surface is slow, resulting to the durability of the droplet for minutes.

According to the discussion above, the self-sustained spherical cap droplet is synergistically controlled by the normalized surface tension difference γ^* and the normalized film thickness th^*. As such, the initial apparent contact angle ACA_{max} can be tuned by modifying either γ^* via the fluid composition or th^* via the thickness of the ethanol film (10–160 μm). As shown in Figure 5, ACA_{max} decreases with either γ^* or th^*. The Weber number ranges from 2 to 6 in Figure 5, yet such variation hardly affects ACA_{max}, as discussed before.

Because the spherical cap configuration is a result of the surface tension gradient, we can introduce a wetting-like toy model to consider only surface tension (for the diagram, see Figure S9a of the Supporting Information). Assuming no mixing at the droplet surface and zero interface tension at the bottom of the spherical cap as a result of full miscibility (reasonably ignored[50−52] and discussed in Figure S9b of the Supporting Information), ACA_{max} is determined by the ethanol fraction of the homogeneous droplet before deposition ϕ_0 via Young's equation $\gamma_e/\gamma(\phi_0) = \cos ACA$. The predicted green line in Figure 5a qualitatively agrees with the experimental data.

This toy model without any parameters provides the unreachable maximum limitation of ACA at certain γ^*, which is 72° for the case of a pure water droplet on a pure ethanol film (Figure 5b). The overpredicted deviation roots from Marangoni convection that increases the ethanol fraction at the droplet surface; therefore, the deviation enlarges with decreasing γ^* or increasing th^*.

CONCLUSION

In conclusion, we have observed the existence of a spherical cap droplet on a continuous liquid film of lower surface tension, despite they are fully miscible and of low viscosities. This spherical cap shape roots from the surface tension gradient or corresponding fraction gradient along the droplet surface. It emerges when the film liquid supplied by Marangoni flow tangential to the droplet surface can be timely diluted by its normal diffusion into the droplet, on the condition that the film thickness can sufficiently suppress the surface flow via large viscous stress. The droplet gradually flattens and collects film liquid before merging into the film after minutes. The increasing rate of the film liquid fraction at the droplet surface is limited by film thickness; therefore, the surface tension gradient decreases slowly. The present finding removes the conventional cognition that droplet coalescence is prompt on fully miscible continuous liquid surfaces. It provides a platform for unidirectional fluidic transport and passive local mixing with the help of Marangoni convection inside of the spherical cap, which could be potentially useful for the design of new types of microfluid systems.

ASSOCIATED CONTENT

Supporting Information

The Supporting Information is available free of charge at https://pubs.acs.org/doi/10.1021/acs.langmuir.1c03457.

Insensitivity of ACA_{max} to film liquid, Weber number, and temperature, simulation of droplet formation, evolution of the colored water droplet on an ethanol thin film for minutes, surface tension of the ethanol aqueous solution plotted against the mass fraction, evolution of ACA according to scaling analysis, and toy model (PDF)

AUTHOR INFORMATION

Corresponding Authors

Jiajia Zhou − *South China Advanced Institute for Soft Matter Science and Technology, School of Emergent Soft Matter, South China University of Technology, Guangzhou 510640,*

https://doi.org/10.1021/acs.langmuir.1c03457
Langmuir 2022, 38, 3993−4000

People's Republic of China; orcid.org/0000-0002-2258-6757; Email: zhouj2@scut.edu.cn

Kai Sun − *State Key Laboratory of Engines, Tianjin University, Tianjin 300072, People's Republic of China;* orcid.org/0000-0001-6409-792X; Email: sunkai@tju.edu.cn

Sheng Meng − *Institute of Physics, Chinese Academy of Sciences, Beijing 100190, People's Republic of China; University of Chinese Academy of Sciences, Beijing 100049, People's Republic of China;* orcid.org/0000-0002-1553-1432; Email: smeng@iphy.ac.cn

Authors

Yutian Shen − *Institute of Physics, Chinese Academy of Sciences, Beijing 100190, People's Republic of China; University of Chinese Academy of Sciences, Beijing 100049, People's Republic of China*

Jiyu Xu − *Institute of Physics, Chinese Academy of Sciences, Beijing 100190, People's Republic of China; University of Chinese Academy of Sciences, Beijing 100049, People's Republic of China;* orcid.org/0000-0002-2628-5492

Mingcheng Yang − *Institute of Physics, Chinese Academy of Sciences, Beijing 100190, People's Republic of China; University of Chinese Academy of Sciences, Beijing 100049, People's Republic of China*

Yongfeng Huang − *Institute of Physics, Chinese Academy of Sciences, Beijing 100190, People's Republic of China; University of Chinese Academy of Sciences, Beijing 100049, People's Republic of China*

Cui Zhang − *Institute of Physics, Chinese Academy of Sciences, Beijing 100190, People's Republic of China; University of Chinese Academy of Sciences, Beijing 100049, People's Republic of China*

Complete contact information is available at: https://pubs.acs.org/10.1021/acs.langmuir.1c03457

Author Contributions

Sheng Meng conceived the project. Yutian Shen designed and performed the experiments. Yutian Shen analyzed the data with the help from Jiyu Xu, Mingcheng Yang, Yongfeng Huang, and Cui Zhang. Kai Sun did the simulations. Kai Sun, Yutian Shen, and Jiajia Zhou did the scaling analysis. The manuscript is prepared by Yutian Shen and Sheng Meng with input from all authors. All of the authors discussed the results and commented on the manuscript.

Notes

The authors declare no competing financial interest.

■ ACKNOWLEDGMENTS

The authors acknowledge financial support from the Ministry of Science and Technology (MOST, Grant 2021YFA1400201) and the National Natural Science Foundation of China (Grants 12025407, 52076147, and 11934003). Yutian Shen thanks Hongxia Lv and Feifei Jia for their help on experiments.

■ ABBREVIATIONS USED

ACA, apparent contact angle; ACA_{max}, initial or maximum apparent contact angle

■ REFERENCES

(1) Chernyy, S.; Järn, M.; Shimizu, K.; Swerin, A.; Pedersen, S. U.; Daasbjerg, K.; Makkonen, L.; Claesson, P.; Iruthayaraj, J. Superhydrophilic polyelectrolyte brush layers with imparted anti-icing properties: Effect of counter ions. *ACS Appl. Mater. Interfaces* **2014**, *6*, 6487−6496.

(2) Cao, L.; Jones, A. K.; Sikka, V. K.; Wu, J.; Gao, D. Anti-Icing superhydrophobic coatings. *Langmuir* **2009**, *25*, 12444−12448.

(3) Guo, P.; Zheng, Y.; Wen, M.; Song, C.; Lin, Y.; Jiang, L. Icephobic/anti-icing properties of micro/nanostructured surfaces. *Adv. Mater.* **2012**, *24*, 2642−2648.

(4) Teh, S. Y.; Lin, R.; Hung, L. H.; Lee, A. P. Droplet microfluidics. *Lab Chip* **2008**, *8*, 198−220.

(5) Chaudhury, M. K.; Whitesides, G. M. How to make water run uphill. *Science* **1992**, *256*, 1539−1541.

(6) Lazar, P.; Riegler, H. Reversible self-propelled droplet movement: A new driving mechanism. *Phys. Rev. Lett.* **2005**, *95*, 136103.

(7) Daniel, S.; Chaudhury, M. K.; Chen, J. C. Fast Drop Movements Resulting from the Phase Change on a Gradient Surface. *Science* **2001**, *291*, 633−636.

(8) Chen, Y. J.; Nagamine, Y.; Yoshikawa, K. Self-propelled motion of a droplet induced by Marangoni-driven spreading. *Phys. Rev. E: Stat., Nonlinear, Soft Matter Phys.* **2009**, *80*, 016303.

(9) Launay, G.; Sadullah, M. S.; McHale, G.; Ledesma-Aguilar, R.; Kusumaatmaja, H.; Wells, G. G. Self-propelled droplet transport on shaped-liquid surfaces. *Sci. Rep.* **2020**, *10*, 14987.

(10) Jiang, Z. W.; Chen, R.; Wu, T.; Ding, H.; Li, E. Q. Contactless transport of sessile droplets. *Phys. Fluids* **2021**, *33*, 112115.

(11) Cira, N. J.; Benusiglio, A.; Prakash, M. Vapour-mediated sensing and motility in two-component droplets. *Nature* **2015**, *519*, 446−450.

(12) Karpitschka, S.; Pandey, A.; Lubbers, L. A.; Weijs, J. H.; Botto, L.; Das, S.; Andreotti, B.; Snoeijer, J. H. Liquid drops attract or repel by the inverted Cheerios effect. *Proc. Natl. Acad. Sci. U. S. A.* **2016**, *113*, 7403−7407.

(13) Liu, C.; Ju, J.; Zheng, Y.; Jiang, L. Asymmetric ratchet effect for directional transport of fog drops on static and dynamic butterfly wings. *ACS Nano* **2014**, *8*, 1321−1329.

(14) Zheng, Y.; Bai, H.; Huang, Z.; Tian, X.; Nie, F. Q.; Zhao, Y.; Zhai, J.; Jiang, L. Directional water collection on wetted spider silk. *Nature* **2010**, *463*, 640−643.

(15) Chen, H.; Zhang, P.; Zhang, L.; Liu, H.; Jiang, Y.; Zhang, D.; Han, J.; Jiang, L. Continuous directional water transport on the peristome surface of *Nepenthes alata*. *Nature* **2016**, *532*, 85−89.

(16) Khodabocus, M. I.; Sellier, M.; Nock, V. Dynamics of thin film under a volatile solvent source driven by a constant pressure gradient flow. *Fluids* **2019**, *4*, 198.

(17) Kim, S.; Kim, J.; Kim, H. Y. Dewetting of liquid film via vapour-mediated Marangoni effect. *J. Fluid. Mech.* **2019**, *872*, 100−114.

(18) Roy, P. K.; Frenkel, M.; Legchenkova, I.; Shoval, S.; Binks, B. P.; Bormashenko, E. Liquid Marble-Induced Dewetting. *J. Phys. Chem. C* **2020**, *124*, 9345−9349.

(19) Li, J.; Li, J.; Sun, J.; Feng, S.; Wang, Z. Biological and Engineered Topological Droplet Rectifiers. *Adv. Mater.* **2019**, *31*, 1806501.

(20) Comanns, P.; Buchberger, G.; Buchsbaum, A.; Baumgartner, R.; Kogler, A.; Bauer, S.; Baumgartner, W. Directional, passive liquid transport: The Texas horned lizard as a model for a biomimetic 'liquid diode'. *J. R. Soc. Interface.* **2015**, *12*, 20150415.

(21) Feng, S. L.; Zhu, P.; Zheng, H.; Zhan, H.; Chen, C.; Li, J.; Wang, L.; Yao, X.; Liu, Y.; Wang, Z. Three-dimensional capillary ratchet-induced liquid directional steering. *Science* **2021**, *373*, 1344−1348.

(22) Song, H.; Chen, D. L.; Ismagilov, R. F. Reactions in droplets in microfluidic channels. *Angew. Chem. Int. Ed.* **2006**, *45*, 7336−7356.

(23) Park, J.; Ryu, J.; Sung, H. J.; Kim, H. Control of solutal Marangoni-driven vortical flows and enhancement of mixing efficiency. *J. Colloid Interface Sci.* **2020**, *561*, 408−415.

(24) Hao, C.; Li, J.; Liu, Y.; Zhou, X.; Liu, Y.; Liu, R.; Che, L.; Zhou, W.; Sun, D.; Li, L.; Xu, L.; Wang, Z. Superhydrophobic-like tunable droplet bouncing on slippery liquid interfaces. *Nat. Commun.* **2015**, *6*, 8986.

(25) Park, K. C.; Kim, P.; Grinthal, A.; He, N.; Fox, D.; Weaver, J. C.; Aizenberg, J. Condensation on slippery asymmetric bumps. *Nature* **2016**, *531*, 78−82.
(26) Wong, T. S.; Kang, S. H.; Tang, S. K.Y.; Smythe, E. J.; Hatton, B. D.; Grinthal, A.; Aizenberg, J. Bioinspired self-repairing slippery surfaces with pressure-stable omniphobicity. *Nature* **2011**, *477*, 443−477.
(27) Orme, B. V.; McHale, G.; Ledesma-Aguilar, R.; Wells, G. G. Droplet Retention and Shedding on Slippery Substrates. *Langmuir* **2019**, *35*, 9146−9151.
(28) Guan, J. H.; Ruiz-Gutiérrez, É.; Xu, B. B.; Wood, D.; McHale, G.; Ledesma-Aguilar, R.; Wells, G. G. Drop transport and positioning on lubricant-impregnated surfaces. *Soft Matter* **2017**, *13*, 3404−3410.
(29) Bico, J.; Tordeux, C.; Quéré, D. Rough wetting. *Europhys. Lett.* **2001**, *55*, 214−220.
(30) Courbin, L.; Denieul, E.; Dressaire, E.; Roper, M.; Ajdari, A.; Stone, H. A. Imbibition by polygonal spreading on microdecorated surfaces. *Nat. Mater.* **2007**, *6*, 661−664.
(31) Blanchette, F.; Bigioni, T. P. Partial coalescence of drops at liquid interfaces. *Nat. Phys.* **2006**, *2*, 254−257.
(32) Blanchette, F.; Messio, L.; Bush, J. W. M. The influence of surface tension gradients on drop coalescence. *Phys. Fluids* **2009**, *21*, 072107.
(33) Hernández-Sánchez, J. F.; Eddi, A.; Snoeijer, J. H. Marangoni spreading due to a localized alcohol supply on a thin water film. *Phys. Fluids* **2015**, *27*, 032003.
(34) Wang, A. B.; Chen, C. C. Splashing impact of a single drop onto very thin liquid films. *Phys. Fluids* **2000**, *12*, 2155−2158.
(35) Chen, N.; Chen, H.; Amirfazli, A. Drop impact onto a thin film: Miscibility effect. *Phys. Fluids* **2017**, *29*, 092106.
(36) Kim, H.; Lee, J.; Kim, T. H.; Kim, H. Y. Spontaneous Marangoni Mixing of Miscible Liquids at a Liquid−Liquid−Air Contact Line. *Langmuir* **2015**, *31*, 8726−8731.
(37) Kim, H.; Muller, K.; Shardt, O.; Afkhami, S.; Stone, H. A. Solutal Marangoni flows of miscible liquids drive transport without surface contamination. *Nat. Phys.* **2017**, *13*, 1105−1110.
(38) Ersoy, N. E.; Eslamian, M. Capillary surface wave formation and mixing of miscible liquids during droplet impact onto a liquid film. *Phys. Fluids* **2019**, *31*, 012107.
(39) Couder, Y.; Fort, E.; Gautier, C. H.; Boudaoud, A. From bouncing to floating: Noncoalescence of drops on a fluid bath. *Phys. Rev. Lett.* **2005**, *94*, 177801.
(40) Savino, R.; Paterna, D.; Lappa, M. Marangoni flotation of liquid droplets. *J. Fluid Mech.* **2003**, *479*, 307−326.
(41) Davanlou, A. The role of liquid properties on lifetime of levitated droplets. *Langmuir* **2016**, *32*, 9736−9742.
(42) Amarouchene, Y.; Cristobal, G.; Kellay, H. Noncoalescing drops. *Phys. Rev. Lett.* **2001**, *87*, 206104.
(43) Deng, Y.; Zheng, X.; Bai, Y.; Wang, Q.; Zhao, J.; Huang, J. Surfactant-controlled ink drying enables high-speed deposition of perovskite films for efficient photovoltaic modules. *Nat. Energy* **2018**, *3*, 560−566.
(44) Dugyala, V. R.; Lama, H.; Satapathy, D. K.; Basavaraj, M. G. Role of particle shape anisotropy on crack formation in drying of colloidal suspension. *Sci. Rep.* **2016**, *6*, 30708.
(45) Wang, J.; Sun, L.; Zou, M.; Gao, W.; Liu, C.; Shang, L.; Gu, Z.; Zhao, Y. Bioinspired shape-memory graphene film with tunable wettability. *Sci. Adv.* **2017**, *3*, No. e1700004.
(46) Derby, B. Inkjet Printing of Functional and Structural Materials: Fluid Property Requirements, Feature Stability, and Resolution. *Annu. Rev. Mater. Res.* **2010**, *40*, 395−414.
(47) Truskett, V. N.; Stebe, K. J. Influence of surfactants on an evaporating drop: Fluorescence images and particle deposition patterns. *Langmuir* **2003**, *19*, 8271−8279.
(48) Sun, K.; Zhang, P.; Che, Z.; Wang, T. Marangoni-flow-induced partial coalescence of a droplet on a liquid/air interface. *Phys. Rev. Fluids* **2018**, *3*, 023602.
(49) Liang, G.; Mudawar, I. Review of mass and momentum interactions during drop impact on a liquid film. *Int. J. Heat Mass Transfer* **2016**, *101*, 577−599.
(50) Truzzolillo, D.; Cipelletti, L. Off-equilibrium surface tension in miscible fluids. *Soft Matter.* **2017**, *13*, 13−21.
(51) Lacaze, L.; Guenoun, P.; Beysens, D.; Delsanti, M.; Petitjeans, P.; Kurowski, P. Transient surface tension in miscible liquids. *Phys. Rev. E: Stat., Nonlinear, Soft Matter Phys.* **2010**, *82*, 041606.
(52) Zoltowski, B.; Chekanov, Y.; Masere, J.; Pojman, J. A.; Volpert, V. Evidence for the existence of an effective interfacial tension between miscible fluids. 2. Dodecyl acrylate-poly(dodecyl acrylate) in a spinning drop tensiometer. *Langmuir* **2007**, *23*, 5522−5531.

https://doi.org/10.1021/acs.langmuir.1c03457
Langmuir 2022, 38, 3993−4000

Supporting information for

Durably self-sustained droplet on a fully miscible liquid film

Yutian Shen,[1,2] Jiyu Xu,[1,2] Mingcheng Yang,[1,2] Yongfeng Huang,[1,2] Cui Zhang,[1,2] Jiajia Zhou*,[3] Kai Sun*,[4] Sheng Meng*[1,2]

[1]Institute of Physics, Chinese Academy of Sciences, Beijing 100190, P. R. China.

[2]University of Chinese Academy of Sciences, Beijing 100049, P. R. China.

[3]South China Advanced Institute for Soft Matter Science and Technology, School of Emergent Soft Matter, South China University of Technology, Guangzhou 510640, China.

[4]State Key Laboratory of Engines, Tianjin University, Tianjin 300072, P. R. China

*Email: zhouj2@scut.edu.cn, sunkai@tju.edu.cn, smeng@iphy.ac.cn

Contents

ACA_{max} is insensitive to film liquid, *Weber* number and temperature

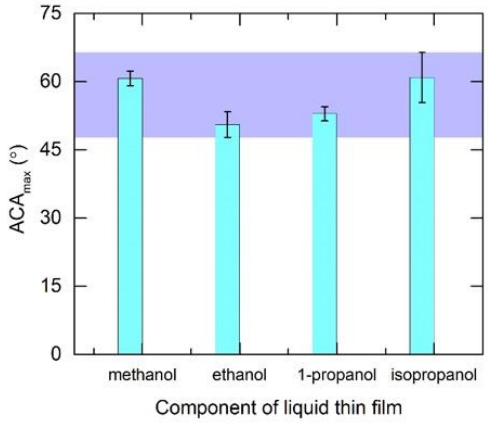

Figure S1 ACA_{max} of water droplet (10 µL) on thin film(thickness, 50 µm) of several liquids (methanol, 1-propanol, and isopropanol) varies slightly (the purple rectangle).

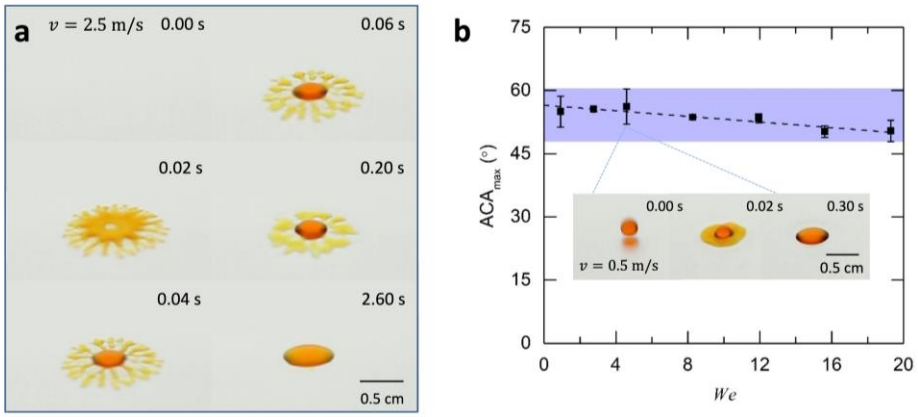

Figure S2 Effect of impacting velocity and *Weber* number on droplet formation ($th^* = 0.03,\ \gamma^* = 0.3,\ Oh \sim 0.005$). (a) Colored water impacting onto thin ethanol film at velocity of 2.5 m/s forms spherical cap droplet. (b) ACA_{max} of water droplets on thin ethanol film at various Weber numbers vary slightly (the purple rectangle). The inset is the case for $We = 4.59$ or impacting velocity of 0.5 m/s.

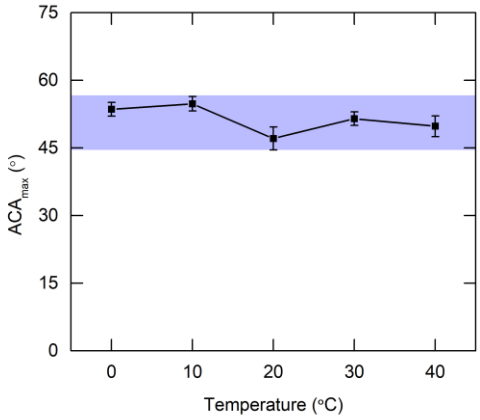

Figure S3 ACA_{max} of water droplet on thin ethanol film at temperature from 0℃ to 40℃ ($th^* = 0.03,\ \gamma^* = 0.3,\ Oh \sim 0.005$) varies slightly (the purple rectangle).

Simulation of droplet formation

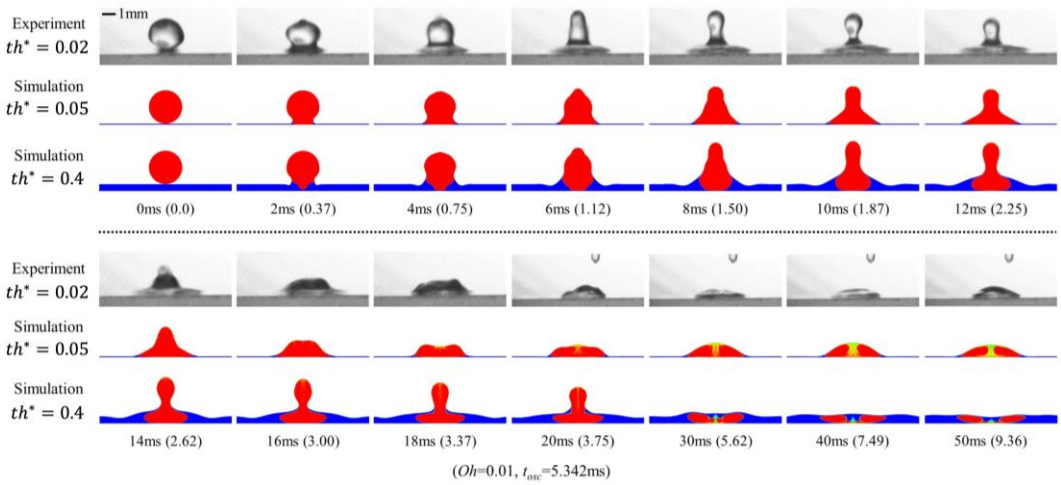

Figure S4 Simulation of ethanol fraction distribution in droplet formation process. Experimental (the first row) and simulated (the second row) side-view of water droplet formation on thin ethanol film. For comparison, water merges into thick ethanol film in the simulation (the third row). Red color fluid donates water, blue for ethanol and intermediate colors for the mixture. All parameters are same as in Fig. 3.

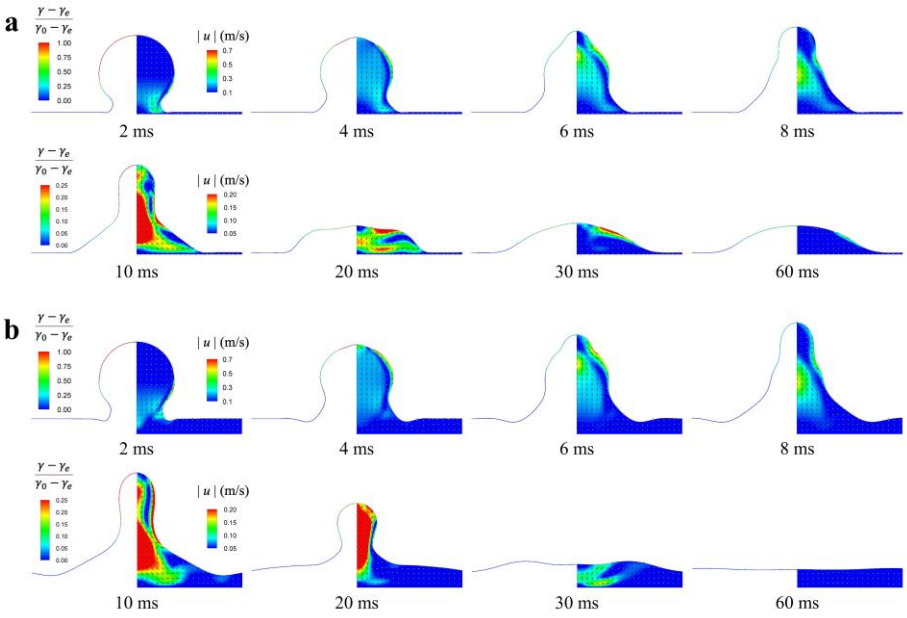

Figure S5 Simulation of surface tension (left side) and flow field (right side) distribution in droplet formation process, where arrows indicate the flow direction. All parameters are same as in Fig. 3.

The numerical methods are as below.

The two-phase flow is modeled by using the phase-field method. The composition C denotes the local volume fraction of liquid in total fluid and its evolution is governed by the *Cahn-Hilliard* equation:

$$\frac{\partial C}{\partial t} + \boldsymbol{u} \cdot \nabla C = M\nabla^2 \mu_C, \tag{1}$$

where $\boldsymbol{u}$ is the fluid velocity, M is the interface mobility, and $\mu_C = \mu_0 - k\nabla^2 C = \partial E_0/\partial C - k\nabla^2 C$ is the chemical potential with E_0 being the bulk free energy and k the gradient factor. The bulk free energy takes a double-well function $E_0 = \beta C^2(1 - C^2)$ and the chemical potential is given by $\mu_C = \beta(4C^3 - 6C^2 + 2C) - k\nabla^2 C$. The surface tension and the interface thickness are determined by $\gamma = \sqrt{2k\beta}/6$ and $\xi = \sqrt{8k/\beta}$, respectively.

In the present simulations, the liquid phase is composed of two miscible

components of water and ethanol and hence $C = C_1 + C_2$. Both two components should have their respective contribution to the *Cahn-Hillard* diffusion, with the proportions being C_1/C and C_2/C, respectively. Therefore, the governing equation of C_1 takes:

$$\frac{\partial C_1}{\partial t} + \boldsymbol{u} \cdot \nabla C_1 = \nabla \cdot (D \nabla C_1) + (C_1/C) M \nabla^2 \mu_c, \tag{2}$$

where the first term on the RHS denotes molecular diffusion with D being the composition diffusivity, and the second term on the RHS describes the partial contribution of this composition to the total *Cahn-Hilliard* diffusion.

The non-dimensional local surface tension γ/γ_w is determined by C_1/C, where γ_w is the surface tension of water. For water/ethanol binary liquid system at room temperature, such dependence can be described by using a fitting form of:

$$\gamma/\gamma_w = a e^{b(C_1/C)} + c e^{d(C_1/C)} + e, \tag{3}$$

where $a = 0.216$, $b = -0.0373$, $c = 0.495$, $d = -0.2996$, and $e = 0.288$. The temporal and spatial variation of surface tension of the liquid-gas interface is realized though k and β. To maintain a uniform interface thickness and a uniform rate of *Cahn-Hilliard* diffusion, we let $k = k_0(\gamma/\gamma_w)$, $\beta = \beta_0(\gamma/\gamma_w)$, and $M = M_0/(\gamma/\gamma_w)$, where k_0, β_0, and M_0 are constants.

Furthermore, the continuity equation and the momentum equation for incompressible flows are:

$$\nabla \cdot \boldsymbol{u} = 0 \tag{4}$$

and

$$\rho\left[\frac{\partial \boldsymbol{u}}{\partial t} + \boldsymbol{u} \cdot \nabla \boldsymbol{u}\right] = -\nabla p + \nabla \cdot [\mu(\nabla \boldsymbol{u} + \nabla \boldsymbol{u}^T)] + \mu_c \nabla C + |\nabla C|^2 \nabla k - (\nabla k \cdot \nabla C)\nabla C, \tag{5}$$

where p is the pressure, and μ is the dynamic viscosity. On the right-hand side of Eq. (5), the third term represents surface tension and the fourth term is the Marangoni stress. The local fluid density and dynamic viscosity are taken linear functions of C by:

$$\rho = \rho_1 C + \rho_g (1 - C) \tag{6}$$

and

$$\mu = \mu_1 C + \mu_g (1 - C) \tag{7}$$

The governing equations of (1), (2), (4), and (5) are solved in their axisymmetric forms. Specifically, Eqs. (1), (4), and (5) are numerically solved by using the lattice Boltzmann method (LBM). In the LBM simulation, one distribution function is used to recover Eq. (1) and another distribution function is used to recover Eqs. (4) and (5). Eq. (2) is not included in the framework LBM but instead solved by using the finite difference method with the 3rd-order Runge-Kutta method for time discretization and the 5th-order WENO scheme for spatial discretization.

In the present phase-filed modelling, the interface *Pèclet* number $Pe_i = \xi \sqrt{\gamma_w/(\rho_w R_0)}/(M_0 \beta_0)$ was fixed at 0.95 to keep the liquid-gas interface close to the equilibrium profile throughout the droplet coalescence process, in which ξ denotes the numerical liquid-gas interface thickness. The droplet radius R_0 was revolved by 300 girds to achieve a balance between computational accuracy and efficiency.

Surface tension of ethanol aqueous solutions plotted against mass fraction

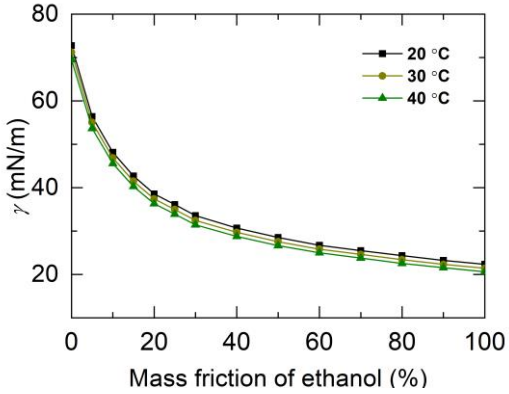

Figure S6 Surface tension of ethanol aqueous solution plotted against mass fraction of ethanol at different temperatures[1]. The fitted relationship between surface tension and ethanol fraction ϕ_e is $\gamma(\phi_e) = [7.37377/(\phi_e + 0.131619) + 16.4361]\, mN/m$.

Evolution of colored water droplet on ethanol thin film for minutes

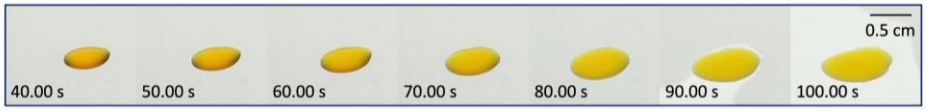

Figure S7 Evolution of colored water droplet on ethanol thin film for minutes. The droplet starts to breakup with ethanol film and be left on solid substrate after 90 s due to evaporation. The photos are in the same process as in Fig. 4c.

Evolution of ACA according to scaling analysis

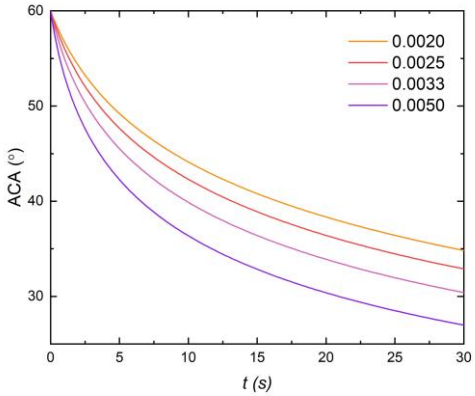

Figure S8 Evolution of ACA of water droplet on thin ethanol film at different th^* according to scaling analysis. $Oh = 0.005$, th^* ranges from 0.002 to 0.005.

Toy model

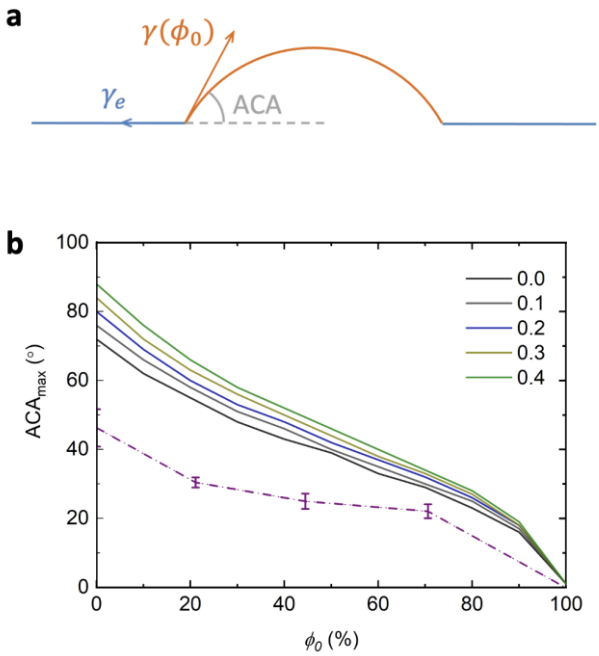

Figure S9 (a) Diagram of the toy model, where $\gamma_e/\gamma(\phi_0) = cosACA$. (b) ACA_{max} of aqueous droplet of various ethanol concentration before deposition ϕ_0 on ethanol film with various supposed interface tension according to the toy model. The interface tension is calculated by surface tension difference between the droplet and ethanol multiplied by 0.1, 0.1, 0.2, 0.3 and 0.4. Factor above 0.4 is nonphysical with interface tension higher than surface tension of ethanol since ethanol and water are completely miscible. The purple scatters are experimental values same as in Fig. 5a.

Reference

1. Vazquez, G.; Alvarez, E.; Navaza, J. M. Surface Tension of Alcohol + Water from 20 to 50 °C. *J. Chem. Eng. Data* **1995**, *40*, 611–614.